AIP Journal of Applied Physics

Fixed photorefractive holograms with maximum index-of-refraction modulation in LiNbO 3 : Fe

Vladimir A. Jerez, Ivan de Oliveira, and Jaime Frejlich

Citation: Journal of Applied Physics **106**, 063116 (2009); doi: 10.1063/1.3223319

View online: http://dx.doi.org/10.1063/1.3223319

View Table of Contents: http://scitation.aip.org/content/aip/journal/jap/106/6?ver=pdfcov

Published by the AIP Publishing

Fixed photorefractive holograms with maximum index-of-refraction modulation in $LiNbO_3$:Fe

Vladimir A. Jerez,[1] Ivan de Oliveira,[2] and Jaime Frejlich[3,a)]
[1]*Grupo de Óptica y Tratamiento de Señales, Universidad Industrial de Santander, Bucaramaga, AA678 Colombia*
[2]*Faculdade de Tecnologia, Unicamp, Limeira, Sao Paulo, 13484-332, Brazil*
[3]*Laboratório de Óptica, IFGW, Unicamp, Campinas, Sao Paulo 13083-970, Brazil*

(Received 6 March 2009; accepted 11 August 2009; published online 24 September 2009)

We report the recording of a fixed good quality transmission hologram in $LiNbO_3$:Fe with maximum index-of-refraction modulation using the simultaneous recording/compensation process at 120 °C in a specially designed setup with $\lambda=514.5$ nm. This process was shown to be reproducible and in good agreement with an already reported theoretical model. The analysis of this recording process showed that material saturation was reached so that the maximum possible fixed index-of-refraction modulation was achieved. From the comparison of theoretical and experimental recording/compensation process data some material parameters (dielectric relaxation time $\tau_M^e \approx 15$ min, saturation space-charge field $E_q=18.8$ kV/cm, and photovoltaic-to-saturation field ratio $E_{ph}/E_q=0.80$) were determined. The diffraction efficiency of this grating was measured using a $\lambda=633$ nm probe laser beam in an independent setup and its actual value computed, taking into account the angular divergence of the probe beam. The good grating performance as an optical Bragg filter was experimentally characterized by independently measuring its angular (approximately 1.2 mrad) and spectral (approximately 0.1 nm) selectivities, both at the probe beam wavelength of 633 nm. © *2009 American Institute of Physics*. [doi:10.1063/1.3223319]

I. INTRODUCTION

Permanent volume holograms or gratings are interesting for different applications and particularly useful as narrow band light filters.[1]

Volume holograms can be fixed in otherwise volatile photorefractive materials by double doping[2] or by temperature processing.[3–8] The latter process, mainly carried out on $LiNbO_3$:Fe, consists of recording an electronic grating followed by its complete compensation at high temperature by nonphotosensitive H^+ ions already present in the material. After that, development with white light proceeds at room temperature in order to (partially) erase the photosensitive electronic grating and allow the nonphotosensitive ionic grating to remain. The larger the electronic grating recorded in the first step, the larger the fixed grating remaining in the final step. The largest possible fixed hologram is obtained by self-stabilized holographic recording[9–12] with unity ($|m|\approx 1$) fringe visibility at high temperature to allow for simultaneous recording and compensation.[13–15]

As far as we know, the best reported results in terms of highly diffracting transmission fixed holograms indicate diffraction efficiencies somewhat higher than 80%,[16] close to 40%,[17] and projected (not actually measured) close to 100%.[11]

In this paper we show that using a recently reported[17] setup one may produce the largest possible fixed index-of-refraction modulation until material saturation is reached in $LiNbO_3$:Fe. This paper is devoted to the analysis of the fixing process and of the resulting fixed grating. We show that the self-stabilized recording/compensation process is reproducible and in good agreement with an already reported[18] theoretical model. From the comparison of the theoretical and experimental results some realistic material parameters are determined. The angular and spectral selectivities of the recorded fixed grating were measured in order to show the high quality of the grating and its practical interest as an optical Bragg filter.

II. THEORY

The theory of fixing by simultaneous recording and compensation at high temperature followed by development at room temperature on $LiNbO_3$:Fe has been studied, among other researchers, by Sturman *et al.*[18] In the present paper we shall use some of Sturman's theoretical developments to analyze our results.

A. Simultaneous recording and compensation

From the paper by Sturman *et al.*[18] the amplitude of the space-charge field due to ions H^+ (as well as due to electrons) at the end of the full compensation process, after recording during a time t_R, is shown to be

$$|E_h(t_R)| \approx |m|E_q(1-e^{-\gamma t_R}), \tag{1}$$

$$\gamma \approx \frac{E_D}{E_q}\frac{1+[Fe^{2+}]/\mathcal{H}_0}{\tau_M^e+\tau_M^h}, \quad E_D \ll E_q, \tag{2}$$

where E_D is the diffusion space-charge field amplitude, E_q is the maximum possible value of the space-charge field amplitude at unity pattern of fringe modulation ($|m|=1$), and $\mathcal{H}_0$ is

a)FAX: +55-19-3521.4145. Electronic mail: frejlich@ifi.unicamp.br.

the spatial average concentration of H^+. The dielectric relaxation times at the high temperature process for electrons and for H^+ are, respectively, τ_M^e and τ_M^h with the former being mainly controlled by the action of light and the latter by the process temperature. We have also assumed that $[Fe^{3+}] \gg [Fe^{2+}]$ and $[Fe^{2+}] \ll \mathcal{H}_0$. In Eq. (1) we have only considered the real part of the exponential constant γ because the imaginary part is only related to phase shifting that disappears at the end of the compensation process in the dark. The parameter γ can be further simplified to

$$\gamma \approx \frac{E_D}{E_q} \frac{1 + [Fe^{2+}]/\mathcal{H}_0}{2\tau_M^e} \tag{3}$$

by assuming that $\tau_M^e \approx \tau_M^h$ because the recording-compensation process temperature is kept high enough for the electronic and the ionic gratings to occur almost simultaneously.

B. Development

After recording the electronic grating during a time t_R (and almost completely compensating it), as described in Sec. II A, and after full compensation in the dark at the operating high temperature, an electronic $E_{sc}(t_R)$ plus an ionic $E_h(t_R)$ grating of equal magnitude and opposite signs $[E_{sc}(t_R) = -E_h(t_R)]$ are obtained. The following development step is carried out under strong uniform white light illumination at room temperature, and during this stage the evolution of the overall space-charge field $E_{sc}^T(t)$ follows the equation[19]

$$E_{sc}^T(t) = E_{sc}(t) + E_h(t_R), \tag{4}$$

where $E_h(t_R)$ is reported in Eq. (1) and $E_{sc}(t)$ is the solution of

$$\frac{dE_{sc}(t)}{dt} + (\omega_R + i\omega_I)E_{sc}(t) + \kappa(\omega_R + i\omega_I)E_h(t_R) = 0, \tag{5}$$

with

$$\omega_R = \frac{1}{\tau_{MW}^e} \frac{1 + K^2 l_s^2}{1 + K^2 L_D^2} \approx \frac{1}{\tau_{MW}^e} = \frac{\sigma_{eW}}{\epsilon\varepsilon_0}, \tag{6}$$

$$\omega_I = -\frac{1}{\tau_{MW}^e} \frac{Kl_{ph}}{(1 + K^2 L_D^2)^2} \frac{[Fe^{3+}]}{[Fe]} \approx -\frac{Kl_{ph}}{\tau_{MW}^e}, \tag{7}$$

$$\frac{[Fe^{3+}]}{[Fe]} \approx 1, \tag{8}$$

$$Kl_{ph} = E_{ph}/E_q, \tag{9}$$

$$\kappa \approx \frac{1}{1 - iKl_{ph}}, \tag{10}$$

where Eqs. (6)–(10) refer to electrons, E_{ph} is the photovoltaic field under white light illumination, and t is the white light development time at room temperature with $E_{sc}(t=0) = -E_h(t_R)$. The parameter L_D is the diffusion length, τ_{MW}^e is the Maxwell relaxation time, σ_{eW} is the conductivity, always due to electrons under white light and at room temperature, and $K = |\vec{K}|$ is the hologram vector value. The approximate relations in Eqs. (6) and (7) are derived from the usual assumptions[20] for the strongly photovoltaic $LiNbO_3$:Fe crystal. The resulting overall field after full development ($t \to \infty$) is

$$E_{sc}^T(\infty) \approx E_h(t_R)(1 - \kappa). \tag{11}$$

C. Diffraction efficiency

Once the hologram is fixed, its diffraction efficiency is measured in an auxiliary setup using a direct high stability extraordinarily polarized He–Ne $\lambda = 633$ nm laser (Spectra Physics model 117A) probe beam. This beam is directed onto the grating at an angle $\theta_0 + \bar{\theta}$, where $\bar{\theta}$ is the shift from the in-Bragg angle θ_0 for this probe beam with a being its angular divergence, all angles have been measured in air. Because of the finite divergence a of the laser beam, an apparent diffraction efficiency is measured as a function of $\bar{\theta}$ that is represented by[21]

$$\bar{\eta}(\bar{\theta}) \equiv P^d(\bar{\theta})/P^{t0}, \tag{12}$$

$$P^d(\bar{\theta}) \equiv \eta(\bar{\theta}) \otimes e^{-2\bar{\theta}^2/a^2} = \int_{\bar{\theta}-\pi/2}^{\bar{\theta}+\pi/2} \eta(\theta) e^{-2(\theta - \bar{\theta})^2/a^2} d\theta, \tag{13}$$

$$P^{t0} \equiv \int_{\bar{\theta}-\pi/2}^{\bar{\theta}+\pi/2} e^{-2(\theta - \bar{\theta})^2/a^2} d\theta = \int_{-\pi/2}^{+\pi/2} e^{-2\theta^2/a^2} d\theta, \tag{14}$$

where P^d is the diffracted power probe beam and P^{t0} is the diffracted plus transmitted power probe beam with the symbol $\otimes$ representing the convolution product and[22]

$$\eta(\bar{\theta}) \equiv \frac{\sin^2 \sqrt{\nu^2 + \xi^2}}{1 + \xi^2/\nu^2} \tag{15}$$

is the slightly out-of-Bragg diffraction efficiency with

$$\nu = \frac{\pi \Delta n d}{\lambda_0}, \tag{16}$$

$$\xi = \frac{K\bar{\theta}d}{2} \frac{\sqrt{1 - \frac{K^2\lambda_0^2}{16\pi^2}}}{\sqrt{n_e^2 - \frac{K^2\lambda_0^2}{16\pi^2}}}, \tag{17}$$

where λ_0 is the wavelength used for measurement and $\bar{\theta}$ is the out-of-Bragg angle, both measured in air, d is the crystal (grating) thickness, and Δn is the index-of-refraction grating modulation as measured with the 633 nm beam that is written as

$$\Delta n = n_e^3 r_{33} |E_{sc}^T(\infty)|/2, \tag{18}$$

where n_e is the extraordinary index of refraction and r_{33} is the corresponding electro-optic coefficient at low frequency. Note that the measured average $\bar{\eta}(\bar{\theta})$ results from a convolution product between the theoretical expression $\eta(\bar{\theta})$ and the angular distribution of light in the probe (measuring) laser beam. The integration in this convolution [see Eqs. (13) and (14)] is actually limited to the angular dimension of the

sensitive area of the photodetectors in the experiment that in the present case is only a few times larger than the angular width a of the laser beam.

D. Angular and wavelength selectivity

Equation (15) is a sharp function centered on θ_0 that represents the rather large angular selectivity ($\Delta\theta_0=\bar{\theta}$) characteristic of short-period thick volume gratings. These gratings also exhibit an associated wavelength selectivity ($\Delta\lambda_0$) that is related to the former one by

$$\frac{\Delta\theta_0}{\Delta\lambda_0}=\frac{\bar{\theta}}{\Delta\lambda_0}=\frac{K}{\sqrt{16\pi^2-K^2\lambda_0^2}}, \tag{19}$$

which is computed from the well known Bragg relation

$$K=\frac{4\pi}{\lambda_0}\sin\,\theta_0. \tag{20}$$

III. EXPERIMENT

The recording was carried out on a 0.9 mm thick $LiNbO_3$:Fe crystal with $[Fe_2^+]/[Fe_3^+]=0.004$, total iron concentration $[Fe]=2\times10^{19}$ cm^{-3}, and total hydrogen ion concentration $[H^+]=2.2\times10^{19}$ cm^{-3} that was provided by Arizmendi from the UAM, Spain. The crystal was short circuited to avoid dc charge accumulation on the sides along $\vec{K}$ with the latter along the photovoltaic axis and contained in the incidence plane (formed by the two incident beams and input crystal plane normal) with symmetrically incident recording beams with a $\pi/2$ angle (outside the crystal) between them. The crystal is fixed in a specially designed copper holder and the whole placed in a homemade temperature-controlled vacuum chamber. The crystal configuration in the setup and the setup itself are the same as already described elsewhere[17] except for the recording wavelength that is now $\lambda=514.5$ nm from the Ar^+ laser.

A. Self-stabilized recording

The recording is carried out under self-stabilized conditions at 120 °C using the temperature-controlled vacuum chamber, extraordinarily polarized recording beams of approximately equal intensity ($\approx$12 mW/cm^2 each) guided into the chamber by polarization maintaining monomode optical fibers from Canadian Instrumentation and Research Ltd. The recording pattern of fringe visibility due to the in-plane (extraordinary) polarization is $\hat{s}\cdot\hat{r}\approx0.8$ with $\hat{s}$ and $\hat{r}$ being the unit polarization vectors of the interfering beams. The resulting spatial period in this geometry is 0.36 μm. The 514.5 nm Ar^+ laser line has a higher power but a much shorter coherence length compared to the previously used solid state 532 nm laser line so that recording was shorter in time and processed at a somewhat higher temperature but required a better interfering beam path difference matching in order not to reduce the pattern of fringe visibility because of limited light coherence. The overall irradiances at the crystal output are[20]

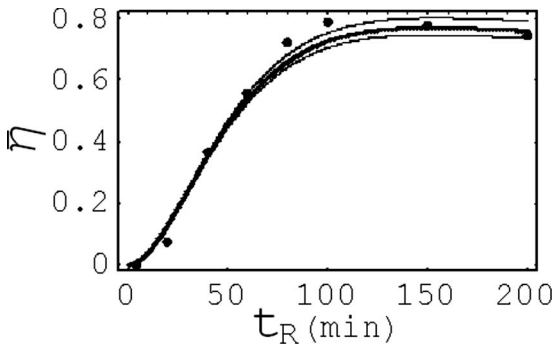

FIG. 1. Directly measured diffraction efficiency (●) vs recording time. The continuous thick curve is the theoretical curve using the parameters $\tau_M^e=15$ min, $E_q=15$ kV/cm, and $a=0.83\pm10\%$ mrad for the probe beam angular divergence, with $Kl_{ph}=0.80$ as reported elsewhere (Ref. 11) for this sample. The two thinner continuous curves are the fitting with the upper and lower 10% limits for a.

$$I_S=I_S^0(1-\eta)+I_R^0\eta+2\hat{s}\cdot\hat{r}\sqrt{\eta(1-\eta)}\sqrt{I_S^0I_R^0}\cos(\varphi+\psi_d\sin\Omega t), \tag{21}$$

$$I_R=I_R^0(1-\eta)+I_S^0\eta-2\hat{s}\cdot\hat{r}\sqrt{\eta(1-\eta)}\sqrt{I_S^0I_R^0}\cos(\varphi+\psi_d\sin\Omega t), \tag{22}$$

with ψ_d and Ω being the amplitude and angular frequency, respectively, of the phase modulation produced in one of the interfering beams and η is the in-Bragg diffraction efficiency during the recording process. All irradiances above are measured behind the sample so that η is free from interface reflections and bulk absorption effects. The expressions of the first and second harmonic terms, arising from phase beam modulation, are, respectively,[20]

$$I^{\Omega}=-4J_1(\psi_d)\hat{s}\cdot\hat{r}\sqrt{\eta(1-\eta)}\sqrt{I_S^0I_R^0}\sin(\varphi), \tag{23}$$

$$I^{2\Omega}=4J_2(\psi_d)\hat{s}\cdot\hat{r}\sqrt{\eta(1-\eta)}\sqrt{I_S^0I_R^0}\cos(\varphi). \tag{24}$$

For strongly photovoltaic materials as is the case of $LiNbO_3$, it is $\varphi\approx\pm\pi/2$ so that $I^{2\Omega}\approx0$ and this latter can be used as error signal to operate the feedback loop in the self-stabilization setup to keep the recording operating at $\varphi=\pm\pi/2$.[10,12,20] As already discussed elsewhere,[17] self-stabilization recording with simultaneous compensation allows recording the largest possible fixed hologram and this is the procedure we follow in this work.

B. Recording evolution

Recording was carried out for different times t_R [see Eq. (4)] and, after hologram fixing, the in-Bragg diffraction efficiency $\bar{\eta}(\bar{\theta}=0)$ was measured, using a direct 633 nm laser probe beam as described in Sec. II C, and plotted as a function of the recording time t_R in Fig. 1. This plot is therefore formed by data from different independent experimental runs and it shows that a maximum was achieved after $t_R\approx120$ min and that no significant changes appear for larger times, thus indicating that the material saturation was reached by that time. Data in Fig. 1 are in good agreement with theory as represented by the continuous curve computed from Eq. (12) taking into account Eqs. (15)–(18) with Eqs.

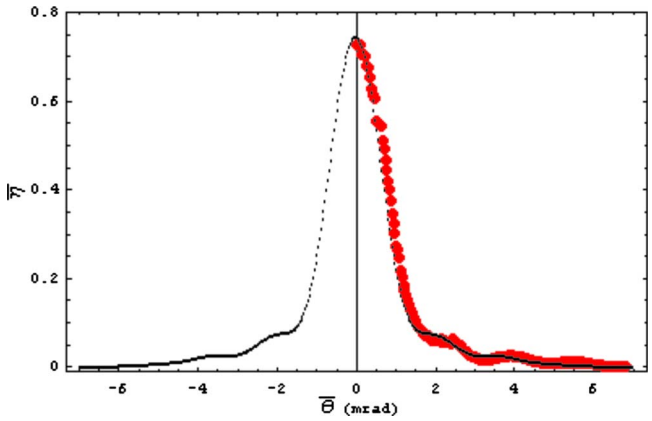

FIG. 2. (Color online) Diffraction efficiency experimental data (●) measured with an extraordinarily polarized 633 nm probe beam and theoretical (dotted) curve leading too $\nu \approx \pi/2 \pm 5\%$ and $a \approx 0.90$ mrad with FWHM ≈ 1.7 mrad. For practical reasons the experimental data were measured only for the positive semiaxis whereas the theoretical curve was displayed on both semiaxes.

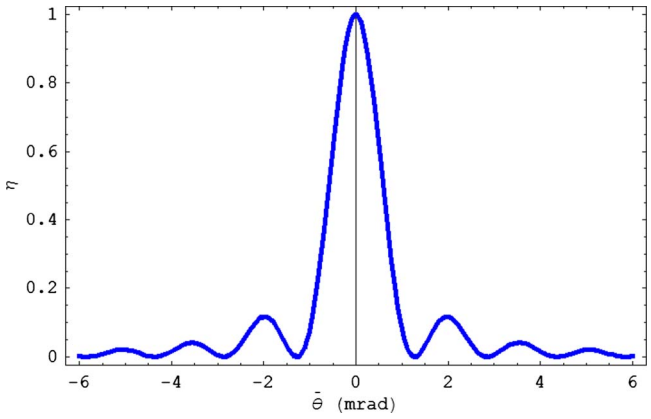

FIG. 3. (Color online) Theoretical η from Eq. (15) as a function of Bragg mismatch angle for $\lambda = 633$ nm using the parameters from the theoretical curve in Fig. 2. The results are $\eta(\bar{\theta}=0) \approx 1$ and FWHM ≈ 1.2 mrad.

(11), (4), and (1) and the parameters $a = 0.83 \pm 10\%$ mrad (manufacturer datasheet indicates 0.8 mrad), $E_q = 18.8$ kV/cm (the estimated theoretical value is 26 kV/cm for this sample), and $Kl_{ph} = 0.80$ (reported to be between 0.73 and 1 for this sample in similar experimental conditions[11]). The good theoretical fitting of these data arising from multiple independent experimental runs also gives some hint about the good reproducibility of the whole process. Diffraction efficiency was always measured at room temperature after development under a strong white light. Such a development could be efficiently carried out only outside the processing chamber and that is why η was always measured with a probe beam in an independent setup but never in the recording setup using the actual recording beam.

C. Actual diffraction efficiency fixed grating

In order to adequately evaluate the diffraction efficiency of the recorded grating it is necessary to recall that the angular divergence of laser probe beams is usually larger than required by the sharp angular selectivity of volume gratings as the present one. In this section we shall take into account the angular width of our probe beam in order to find out the actual diffraction efficiency value of our grating.

Once the maximum measured diffraction efficiency $\bar{\eta}(\bar{\theta}=0) \approx 0.75$ was achieved, the diffraction efficiency was measured as a function of the out-of-Bragg angle $\bar{\theta}$ and plotted in Fig. 2. Because of the large number of data to be measured for plotting in Fig. 2, the sample was illuminated with the strong development white light source after each measurement for the different $\bar{\theta}$ in order to keep comparable steady state development conditions. These data (●) were compared with the theoretical expression for $\bar{\eta}(\bar{\theta})$ (continuous curve) and from this comparison the parameters $\nu \approx \pi/2$ rad (and associated index-of-refraction modulation $\Delta n \approx 3.1 \times 10^{-4}$) and $a \approx 0.9$ mrad (not much different from the $0.83 \pm 10\%$ reported in Sec. III B) were obtained. From these parameters the deconvoluted $\eta(\bar{\theta})$ was computed and plotted in Fig. 3, showing a maximum $\eta(0) \approx 1$ with full width at half maximum (FWHM) ≈ 1.2 mrad. As explained in Sec. III B η was always measured in an auxiliary setup that was provided with the necessary rotating and translating mechanical stages that were lacking in our vacuum chamber.

D. White light filtering

The performance of the fixed grating as a Bragg filter was directly evaluated by filtering out some selected wavelengths from a white light source placed far away from the grating in order to ensure an illumination with a reasonable low degree of angular divergence that was here better than ≈2 mrad. The monochromaticity of the diffracted light was measured with an HR400 model high resolution minispectrometer from Ocean Pacific, and the corresponding spectra are shown in Fig. 4, where the numbers by the side of each spectral line are the corresponding estimated FWHM values. Note that the value for $\lambda \approx 633$ nm is 1.6 nm whereas the resolution of our spectrometer was estimated (as measured on the probe beam itself) to be ≈1.5 nm at this wavelength. Wavelength and angular Bragg conditions mismatching for diffraction are related so that the angular detuning corresponding to $\Delta\lambda_0 \approx 0.1$ nm can be computed from Eq. (19) to be $\Delta\theta_0 = \bar{\theta} \approx 0.3$ mrad, with $\lambda_0 = 633$ nm, $K = 17.3$ μm^{-1},

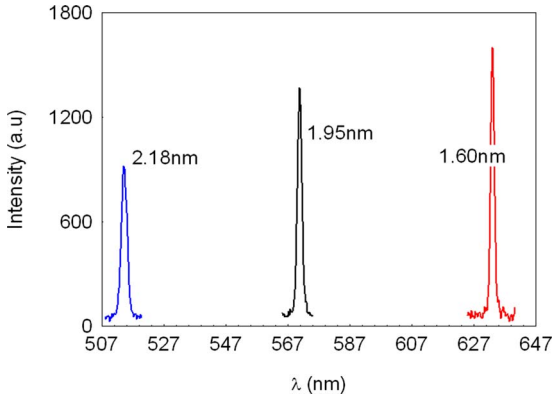

FIG. 4. (Color online) Light diffracted from a white light source using the fixed grating. The numbers represent the FWHM for the three different wavelengths shown. The resolution of the spectrometer at 633 nm is FWHM = 1.5 nm.

and $n_e=2.2$. This FWHM≈ 0.3 mrad value is roughly fourfold lower than the value computed from the actual (deconvoluted) diffraction efficiency data in Fig. 3 but we should nevertheless consider the rather large uncertainty on $\Delta\lambda_0$ due to the fact that the measured value is too much close to the resolution limit of our instrument. Note also that the spectra in Fig. 4 become smaller and wider for decreasing wavelengths. The smaller size is due to the fact that we are using an incandescent white light source with higher infrared and lower ultraviolet contents. The increase in $\Delta\lambda_0$, on the other hand, is a consequence of Eq. (19), showing that for a constant $\bar{\theta}$ the width for 515 nm is almost 45% larger than for 633 nm; for a more quantitative explanation, however, the response of the spectrometer should have to be also taken into account.

IV. CONCLUSIONS

The present paper does provide additional experimental support for the theoretical developments on hologram fixing in $LiNbO_3$:Fe and at the same time unequivocally demonstrates the good performance and reproducibility of our experimental setup.

Although highly diffracting fixed gratings have been obtained without self-stabilized recording techniques too, the use of this technique ensures successful and reproducible first attempt results for all and any experimental run. The high degree of reproducibility in our experiments allowed us to carry out successive fixing experiments with increasing recording times as required for the data shown in Fig. 1. Such a good performance is certainly due to the use of self-stabilized holographic recording that allows long-term recording times with minimum perturbation. It is also worth pointing out the importance of using monomode polarization maintaining optical fibers to guide spatially filtered, adequately polarized recording beams into the vacuum chamber with minimum wavefront distortion. Fibers also allow to mechanically uncouple the recording chamber (that is here placed over a thick polyurethane foam layer) from the laser beam generator that is a source of vibration because of its running water cooling system.

Another relevant practical achievement is not only the high diffraction efficiency ($\approx$100%) achieved here but the fact that we are able to record as large an index-of-refraction modulation as the nature (Fe doping and degree of oxidation) of the sample will allow to. By adequately selecting the sample thickness and nature, any diffraction efficiency can be obtained.

The good quality of the fixed grating here is characterized both in terms of angular and wavelength selectivities, and the role of the probe beam is stressed. In fact, we show that the angular spectrum of the probe beam must be taken into account for accurately characterizing relatively thick short-period gratings as the present one. Otherwise erroneous results may result as was the case of the directly measured 75% diffraction efficiency that turned out to be $\approx$100% after adequate data processing.

[1] R. Müller, M. T. Santos, L. Arizmendi, and J. M. Cabrera, J. Phys. D: Appl. Phys. **27**, 241 (1994).
[2] K. Buse, A. Adibi, and D. Psaltis, Nature (London) **393**, 665 (1998).
[3] J. Amodei and D. Staebler, Appl. Phys. Lett. **18**, 540 (1971).
[4] L. Arizmendi, J. Appl. Phys. **65**, 423 (1989).
[5] S. Breer, K. Buse, K. Peithmann, H. Vogt, and E. Krätzig, Rev. Sci. Instrum. **69**, 1591 (1998).
[6] N. Korneev, H. Veenhuis, K. Buse, and E. Krätzig, J. Opt. Soc. Am. B **18**, 1570 (2001).
[7] S. W. McCahon, D. Rytz, G. C. Valley, M. B. Klein, and B. A. Wechsler, Appl. Opt. **28**, 1967 (1989).
[8] A. Yariv, S. Orlov, G. Rakuljik, and V. Leyva, Opt. Lett. **20**, 1334 (1995).
[9] A. A. Freschi and J. Frejlich, J. Opt. Soc. Am. B **11**, 1837 (1994).
[10] I. de Oliveira, J. Frejlich, L. Arizmendi, and M. Carrascosa, Opt. Commun. **229**, 371 (2004).
[11] I. de Oliveira, J. Frejlich, L. Arizmendi, and M. Carrascosa, Opt. Commun. **247**, 39 (2005).
[12] P. M. Garcia, K. Buse, D. Kip, and J. Frejlich, Opt. Commun. **117**, 235 (1995).
[13] G. A. Rakuljic, Opt. Lett. **22**, 825 (1997).
[14] S. Breer, K. Buse, and F. Rickermann, Opt. Lett. **23**, 73 (1998).
[15] J. Frejlich, I. de Oliveira, L. Arizmendi, and M. Carrascosa, Appl. Opt. **46**, 227 (2007).
[16] A. Méndez and L. Arizmendi, Opt. Mater. (Amsterdam, Neth.) **10**, 55 (1998).
[17] J. von Bassewitz, I. de Oliveira, and J. Frejlich, Appl. Opt. **47**, 5315 (2008).
[18] B. I. Sturman, M. Carrascosa, F. Agullo-Lopez, and J. Limeres, Phys. Rev. B **57**, 12792 (1998).
[19] I. de Oliveira, J. Frejlich, L. Arizmendi, and M. Carrascosa, Opt. Lett. **28**, 1040 (2003).
[20] J. Frejlich, *Photorefractive Materials: Fundamental Concepts, Holographic Recording, and Materials Characterization* (Wiley-Interscience, New York, 2006).
[21] I. de Oliveira and J. Frejlich, J. Opt. A, Pure Appl. Opt. **5**, S428 (2003).
[22] H. Kogelnik, Bell Syst. Tech. J. **48**, 2909 (1969).